The Interface between Caldesmon Domain 4b and Subdomain 1 of Actin Studied by Nuclear Magnetic Resonance Spectroscopy†

Yuan Gao,‡ Valerie B. Patchell,§ Pia A. J. Huber,|| Oneal Copeland,⊥ Mohammed El-Mezgueldi,⊥ A. Fattoum,# Bernard Calas,# Peter B. Thorsted,‡,⊥ Steven B. Marston,*,⊥ and Barry A. Levine‡,§

School of Biochemistry and Division of Medical Science, School of Medicine, University of Birmingham, Birmingham, B15 2TT, United Kingdom, Imperial College School of Medicine at NHLI, London, SW3 6LY, United Kingdom, Division of Medical and Molecular Genetics, King's College, Guy's Hospital, London SE1 9RT, United Kingdom, and CRBM, CNRS, INSERM U249, F-34090 Montpellier, France

Received June 16, 1999; Revised Manuscript Received August 26, 1999

ABSTRACT: The ability of caldesmon to inhibit actomyosin ATPase activity involves the interaction of three nonsequential segments of caldesmon domain 4 (amino acids 600−756) with actin. Two of these contacts are located in the C-terminal half of this region of caldesmon which has been designated domain 4b (658−756). To investigate the spatial relationship between the two sites and to determine whether their corresponding contacts on actin are sequentially distinct, we have used NMR spectroscopy to compare the actin binding properties of the minimal inhibitory peptide LW30 comprising residues 693−722 with those of the recombinant domain 4b constructs 658C (658−756) and Cg1 (a mutant of 658C in which the sequence $_{691}$Glu-Trp-Leu-Thr-Lys-Thr$_{696}$ is changed to Pro-Gly-His-Tyr-Asn-Asn). Cg1 retains dual-sited actin attachment but displays lowered actin affinity. In the presence of tropomyosin, domain 4b−actin contacts were stronger but not qualitatively different, indicating that tropomyosin affected the conformational equilibrium of caldesmon binding. Simultaneous dual-sited attachment of domain 4b to actin is enabled by the conformational properties of the site-spanning sequence common to 658C, Cg1, and LW30 as reflected in the corresponding NOE and other NMR spectral parameters. A backbone turn region ($_{713}$Gly-Asp-Val-Ser$_{716}$) preceded by an extended segment (Ser$_{702}$-Pro-Ala-Pro-Lys-Pro) acts to constrain the relative disposition of the flanking actin contact sites of domain 4b. In tests with a library of actin peptides, only the C-terminus, 350−375, bound to 658C and LW30. The use of Cu^{2+} as a paramagnetic spectral probe bound to the unique His-371 provided evidence of a well-defined geometry for the complex between LW30 and actin residues 350−375 with the N-terminal, site B of domain 4b close to the C-terminal residues of actin. The data are discussed in the context of the potentiation of inhibitory activity by tropomyosin.

The regulation of contractile response in smooth muscle is considered to involve the Ca^{2+}-mediated inhibition of actomyosin ATPase by caldesmon as a mechanism which modulates the primary regulation via phosphorylation−dephosphorylation of the myosin light chain (*1*−*4*). In the test tube, caldesmon inhibition of actomyosin ATPase at in vivo stoichiometries is dependent upon tropomyosin also being present on the thin filament (*5*, *6*). Moreover, low concentrations of caldesmon (10 nM) inhibit actin−tropomyosin filament movement over HMM in the in vitro motility assay (*7*−*9*). Together these observations suggest that caldesmon influences the functional equilibrium of the thin filament in a manner mediated by tropomyosin by a mechanism analogous to inhibition by striated muscle troponin (*10*−*12*).

The resolution of the surface(s) of contact between actin and caldesmon is important in the analysis of the structural basis for this regulatory mechanism in smooth muscle. Targeted mutagenesis has proved a useful tool for elucidating the biochemical characteristics associated with different regions of its primary structure, and a variety of experimental approaches have thereby shown that the calcium-sensitive inhibitory properties of caldesmon are localized within the C-terminal region, domain 4, of the molecule (*13*−*15*). A number of recombinant protein fragments derived from the C-terminal half of domain 4 of caldesmon (domain 4b) are found to be effective tropomyosin-potentiated suppressors of actomyosin ATPase activity (*16*, *17*). Two associated actin binding segments flanking residues 692 and 722 in domain 4b have been independently identified by mutagenic, biochemical, and spectroscopic studies (*13*, *18*, *19*). Studies of the interaction of F-actin with the entire domain 4b (residues

† This work has been supported by grants from the British Heart Foundation (PG97/143 and PG94/069) and the Wellcome Trust (052047).

* Address correspondence to this author. Telephone: +44 (0)207 351 8147. Fax: +44 (0)207 823 3392. E-mail: S.Marston@ic.ac.uk.
‡ School of Biochemistry, University of Birmingham.
§ Division of Medical Science, University of Birmingham.
|| King's College, Guy's Hospital.
⊥ Imperial College School of Medicine at NHLI.
CRBM, CNRS.

10.1021/bi991383k CCC: $18.00
Published on Web 10/30/1999

658−756 of chicken gizzard caldesmon construct 658C) have correlated the tropomyosin-potentiated inhibitory ability of this recombinant fragment with its double-sited docking to F-actin (*18*). Inhibitory properties are not found, however, to be retained by peptides with sequences matching only one of the two proposed actin binding segments of domain 4b, suggesting that regulatory interaction with actin indeed involves a combination of contacts. This hypothesis is further supported by the observation that a short peptide (residues 693−722, LW30) which contains only the two proposed actin contact sites and the intervening sequence does act as an inhibitor of actomyosin ATPase activity (*19*).

To investigate the spatial relationship between the two sites of domain 4b and to determine whether their corresponding contacts on actin are sequentially distinct, we have used NMR spectroscopy to compare the actin binding properties of peptide LW30 with those of the recombinant domain 4b constructs 658C and Cg1 (a mutant of 658C in which the sequence $_{691}$Glu-Trp-Leu-Thr-Lys-Thr$_{696}$ is changed to Pro-Gly-His-Tyr-Asn-Asn). Cg1 retains dual-sited actin attachment but displays lowered actin affinity (*18*). The ^{15}N and ^{1}H resonance chemical shifts and NOE data sets of construct 658C reflected the overall flexibility of the conformation of domain 4b of chicken gizzard caldesmon. One segment notably constrained, residues 702−707, adopts an extended backbone conformation whose rigidity and span derives from the trans configuration adopted by this $(X\text{-}Pro)_3$ sequence. This region of the molecule separating the two actin binding sites involving Trp-692 and Trp-722 was observed to not participate in making docking contacts with actin. In view of this and in light of the simultaneous association with F-actin apparent for the two actin binding regions, we have focused on the structural properties of the residue span that links the two sites.

We have undertaken a two-dimensional NMR study of the peptide LW30 (residues 693−722), comprising the segment linking the two sites and previously shown to possess inhibitory activity that increases in the presence of tropomyosin (*19*). This study identified a backbone turn region characteristic of the parent molecule which acts to constrain the relative disposition of the two actin contact sites. Further, interaction studies using a library of actin peptides have identified a region of actin subdomain 1 contributing to the inhibitory outcome of these caldesmon−actin contacts. The data are discussed in the context of the potentiation of inhibitory activity by tropomyosin with reference to the actin interaction of the inhibitory region of striated muscle troponin I.

MATERIALS AND METHODS

To test the relative contribution of each of the two actin binding segments to the interaction of domain 4b peptide 658C (658−756) with actin, we mutated residues 691−696, leaving the fragment with just one tryptophan at position 722. The mutation of the sequence within site B included the replacement of the hydrophobic residue tryptophan by glycine; charge changes; the introduction of two unique residues, histidine and tyrosine, to aid NMR characterization; and the introduction of a proline residue aiming to influence binding to this site by affecting the ability of this sequence to adopt a helical configuration. Caldesmon peptides 658C and Cg1 were obtained by bacterial expression in the pMW172 plasmid/BL21(DE3) cell system and purified as previously described (*17*, *18*). Solutions of the caldesmon fragments were prepared for the NMR experiments from samples lyophilized from either $^{1}H_2O$ or $^{2}H_2O$ at a concentration of 1−3 mM, and spectra were acquired either in 90% $^{1}H_2O$/10% $^{2}H_2O$ or in 99.9% $^{2}H_2O$ using 25 mM deuterated (d_{11}) Tris as buffer. No spectral changes suggestive of protein aggregation or denaturation were detected in spectra obtained over the concentration range 0.2−3 mM and pH range of 5−8.

The LW30 peptide comprising chicken gizzard caldesmon residues 693−722, the troponin I inhibitory peptide (rabbit skeletal residues 96−116), and the actin peptides were synthesized and purified as previously described (*19*). The composition and purity of the peptides were confirmed by mass and NMR spectroscopy. The ^{1}H NMR spectra of the LW30 peptide were invariant over the concentration range from 0.05 to 5×10^{-3} M, and the narrow line widths observed were taken to indicate the absence of aggregation.

Actin was prepared by the method of Spudich and Watt (*20*) and stored as the freeze-dried protein. Before use, 12 mg of the powder was dissolved in 1 mL of a buffer solution at pH 8.0 containing 5 mM triethanolamine hydrochloride, 0.2 mM $CaCl_2$, 0.2 mM ATP, and 0.2mM DTT.[1] The actin was fully polymerized by dialyzing against this buffer solution for 3 h. Any insoluble material was removed by centrifugation in a microcentrifuge (6500 rpm) for 10 min. The supernatant containing G-actin was dialyzed against the same buffer solution containing 2 mM $MgCl_2$ and 50 mM KCl. The polymerized actin solution was then dialyzed with gentle shaking into 5 mM phosphate buffer, pH 7.6, made up in $^{2}H_2O$. Protein concentrations were determined by the method of Lowry in the case of actin and using the calculated extinction coefficients $\epsilon^{280} = 17\,550$ M^{-1} cm^{-1} for 658C and $\epsilon^{280} = 5850$ M^{-1} cm^{-1} for Cg1. Binding titrations were carried out at 500 MHz by addition of small aliquots of a 10 mg/mL solution of F-actin at a sample pH of 7.6 and at 285 K. Additions were made using a positive displacement pipet to samples in Eppendorf tubes. Efficient mixing was achieved with a whirlimixer, and the solution was then transferred into the NMR sample tube for spectral analysis.

One-dimensional ^{1}H NMR spectra were acquired using a 10 ppm sweep width and typically comprised 128 transients of 16K data points. Two-pulse spin−echo spectra were obtained using a $(180-t-90-t)$ sequence with a delay time $t = 60$ ms and an interpulse delay of 2.5 s to allow for signal recovery with presaturation of the solvent resonance during this relaxation delay. Standard, two-dimensional (2D) total correlation spectroscopy (TOCSY) and nuclear Overhauser effect spectroscopy (NOESY) experiments (250 and 500 ms mixing times) were used for the assignment of resonances of the LW30 peptide.

Interproton distance constraints were classified into four groups with upper band distances of 2.8, 3.3, 4.0, and 4.5 Å, respectively. Structural calculations were carried out using X-PLOR 3.8.5.1 (*21*) with pseudo-atom corrections added

[1] Abbreviations: DTT, 1,4-dithio-DL-threitol; NOE, nuclear Overhauser enhancement; NOESY, nuclear Overhauser enhancement spectroscopy; TOCSY, total correlation spectroscopy.

where appropriate and averaging applied to NOEs involving nonstereospecifically assigned protons. The HA, CA, N, NH, CB*, and CG* atoms of each residue of the LW30 sequence comprising residues 709−720 were embedded using the distance geometry (dg-ab-embed) routine. The remaining atoms were ordered by template fitting and the atomic coordinates allowed to evolve under the applied distance constraints. The 100 structures generated were analyzed by using X-PLOR routines, and those with total NOE distance constraint violations exceeding 1 Å or with wrong-handed geometry were discarded. Final structures were subjected to the X-PLOR Accept routine with a violation threshold for NOEs of 0.5 Å and dihedral angles of 5°.

Samples for 2D experiments typically comprised 1 mM LW30 peptide, pH 5.6 and/or pH 7.6, dissolved in 90% H_2O/10% ^2H_2O, and spectra were collected at 285 K. The $^3J_{HNH\alpha}$ coupling constants for LW30 were obtained directly from the resolved amide protons in the 1D spectra acquired with a digital resolution of 0.21 Hz/point. The experimental protocol and conditions used for the acquisition at 600 MHz of the homonuclear and ^{15}N-edited spectra of the caldesmon constructs 658C and Cg1 have been previously described (*18*).

RESULTS

Both Termini of LW30 (Caldesmon Residues 693−722) Make Contact with Actin. The actin binding properties of the synthetic peptide LW30, caldesmon residues 693−722, were studied by NMR to monitor any spectral perturbations resulting from actin interaction. Prerequisite to such analysis is the correlation of the various resonances with specific groups along the peptide chain. The proton resonance spin system for LW30 was traced through TOCSY spectra (Figure 1A), and complete sequence-specific resonance assignment was achieved primarily using $i \rightarrow i+1$ NOE connectivities (Figure 1B). The signal assignments for the different residues of LW30 are presented as supporting data (see Supporting Information).

Titration of peptide LW30 with F-actin led to the marked perturbation of a very restricted set of resonances. The signals of groups most affected by complex formation are identified in Figure 2 and are seen to derive from both the N-terminal (e.g., Thr-694 and -696) and the C-terminal (e.g., Leu-721 and Trp-722). Readily resolvable resonances of residues in the region spanning the binding sites are observed to remain relatively unaffected (e.g., Asn-700, Ala-704, Asp-709, Arg-711, Asp-714, and Val-715; Figure 2). This indicates that these residues are not directly involved in the interaction of LW30 with F-actin. In contrast, the progressive line broadening of the resonances of Thr-694, Thr-696, Leu-721, and Trp-722 occurred in parallel with increasing extents of complex formation and is indicative of a dual-sited interaction of LW30 with F-actin, similar to that previously observed with the longer peptide 658C(658−756) (*18*).

Tropomyosin Enhances the Affinity of the Two Actin Binding Sites. In thin filaments, the inhibitory effect of caldesmon on actin activation of myosin ATPase is greatly enhanced by the presence of tropomyosin bound to actin (*22*). Tropomyosin has been shown to increase the affinity of caldesmon and active peptides derived from it for actin (*13, 17, 19, 22*). We therefore investigated the effect of tropomyosin on the LW30 peptide interaction with actin. The presence of tropomyosin at a tropomyosin to actin mole ratio of 1:7 increased the degree of association between LW30 and F-actin as judged by the enhanced relaxation of side chain groups of the terminal contact residues (Thr-694, Thr-696, Leu-721, Trp-722). Enhanced relaxation was detected as changes of resonance amplitudes in two-pulse spin−echo experiments (Figure 3). These spectral differences are not marked and therefore indicate a relatively small alteration in actin affinity.

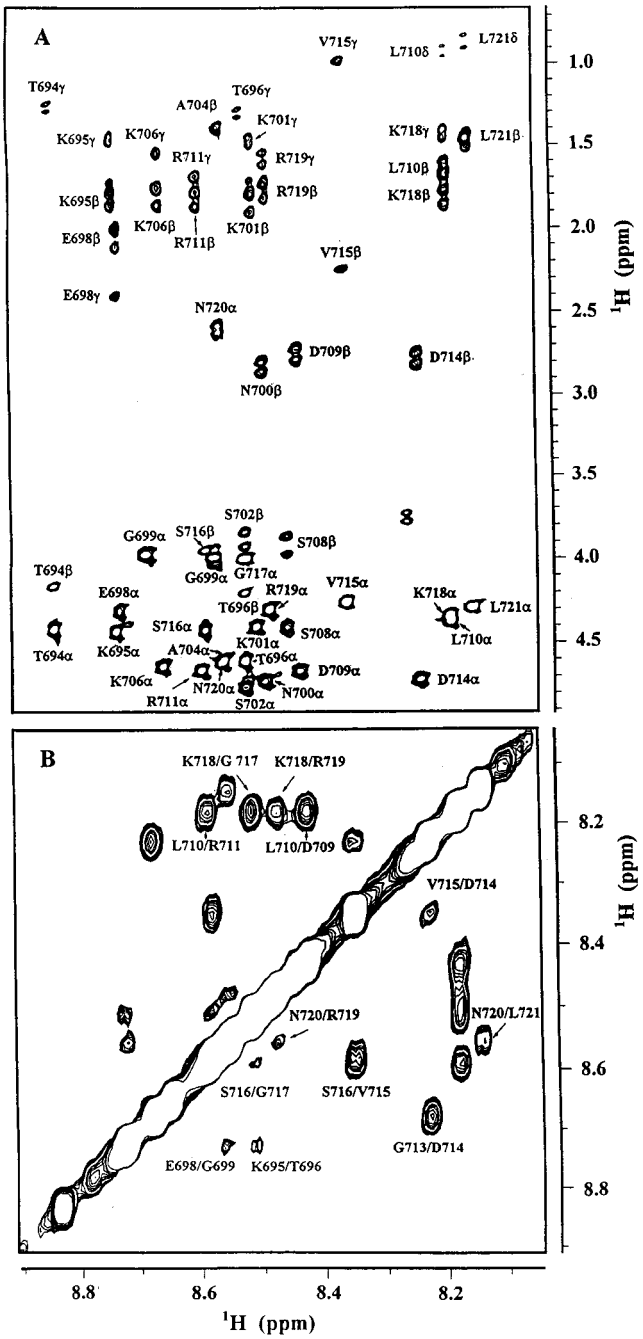

FIGURE 1: (A) Amide spectral region of the ^{1}H 2D TOCSY spectrum of LW30 (1 μM, pH 5.7, $T = 285$ K) showing the signal assignments. (B) Amide spectral region of the ^{1}H 2D NOESY spectrum of LW30 under the same solution conditions. Cross-peaks for the various d_{NN} proximities are labeled as are the sequential $d_{\alpha N}$ and longer range cross-peaks for residues 713−717 whose relative intensities are represented in the NOE data compilation shown in Figure 5A.

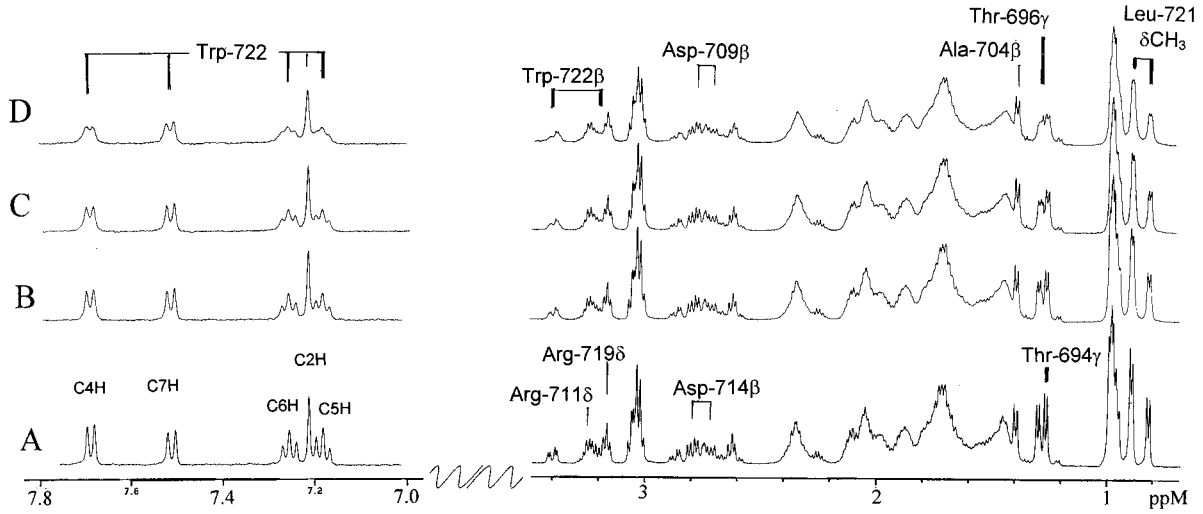

FIGURE 2: Proton spectrum of LW30 at different stages of titration with F-actin. (A) 400 μM LW30, pH 7.5, $T = 295$ K; (B−D) in the presence of 5, 15, and 25 μM F-actin, respectively. The signals of LW30 markedly affected by interaction are indicated by boldface vertical lines while other assignments are shown with lightface vertical lines.

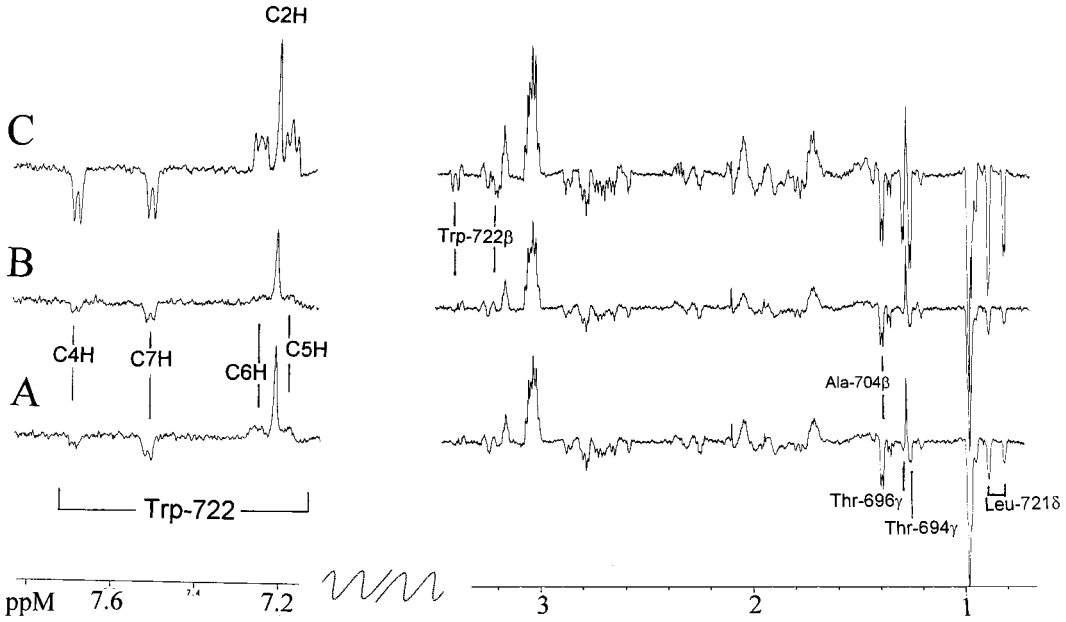

FIGURE 3: Two-pulse (90−t−180−t) spin−echo ^{1}H spectrum of LW30 ($t = 60$ ms). (A) 250 μM LW30 in the presence of 12 μM F-actin, pH 7.6, $T = 295$ K. (B) Upon addition of 2 μM tropomyosin into solution, pH 7.6, $T = 295$ K. (C) Upon further addition of 12 μM troponin I inhibitory peptide, pH 7.6, $T = 295$ K, showing the reduction in signal amplitude in the presence of tropomyosin and the marked increase in signal intensity that results from displacement of LW30 by the troponin I peptide (cf. spectra C and A).

Competition experiments using the inhibitory peptide of troponin I that binds to the N-terminus of actin (*23*) showed that the interaction of LW30 with F-actin−tropomyosin was readily dissociated by the peptide. The addition of very low concentrations of the troponin I peptide (a mole ratio of 1:20 relative to LW30) reversed the spectral changes in LW30, indicating the simultaneous displacement of both its actin contacts. This displacement by the short (20 residue) troponin I peptide was also observed with the larger 658C peptide and reinforces the conclusion that LW30 makes homologous dual contacts with actin. We therefore went on to probe the influence of tropomyosin on the binding of caldesmon domain 4b to actin using the Cg1 mutant peptide.

The potentiation by tropomyosin of the ATPase inhibitory effect of caldesmon domain 4b and its analogue, LW30, was also observed with the Cg1 mutant (the sequence around actin binding site B; $_{691}$Glu-Trp-Leu-Thr-Lys-Thr$_{696}$ is changed to Pro-Gly-His-Tyr-Asn-Asn) (*18*). The two actin binding sites of Cg1 displayed differing apparent affinity; therefore, Cg1 provided the means for investigating the structural basis for the enhancement of actin affinity by monitoring the influence of tropomyosin on each of the two sites. His-693/Tyr-694 and Trp-722 act as separate NMR spectral reporter groups for each site. While interaction of Cg1 with tropomyosin was not be detected in separate titrations, the addition of actin−tropomyosin to Cg1 revealed that the two sites displayed similar actin affinity in the presence of tropomyosin. The progressive perturbation of the signals of Trp-722 induced by increasing complex formation with actin−tropomyosin (mole ratio 7:1) was observed to virtually coincide with that observed for His-693 and Tyr-694, consistent with an estimated upper limit of a 2-fold difference

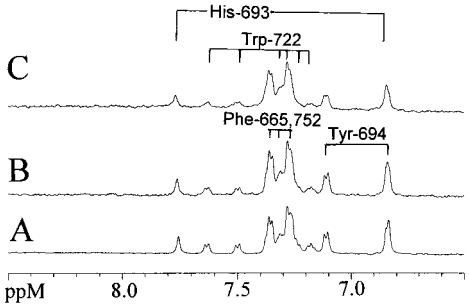

FIGURE 4: Aromatic region of the ^{1}H spectrum of Cg1 showing the signals of His-693, Tyr-694, and Trp-722 that act as distinct reporters for the two actin binding regions. (A) 220 μM Cg1, pH 7.6, T = 295 K. (B and C) Upon addition of actin−tropomyosin (7:1 mole ratio) at a concentration of 7 and 13 μM, respectively. Note the progressive broadening of the side chain signals of Trp-722 that is almost paralleled by the broadening of the resonances of His-693 and Tyr-694.

in affinity between the two sites (Figure 4). The concentration of actin−tropomyosin required to elicit these spectral changes in Cg1 was notably lower than that needed upon complex formation with actin alone, confirming that tropomyosin enhanced the affinity for actin of both actin binding sites of caldesmon domain 4b. Further, as found upon complex formation with actin alone, dual-sited interaction with actin−tropomyosin occurs with restricted segments of domain 4b and does not directly involve other regions of the molecular structure. Signals from the site-spanning residues and the terminal region remain relatively unaffected (e.g., Phe-665 and Phe-752; Figure 4). It is therefore likely that tropomyosin increases the accessibility on F-actin for the dual-sited binding of domain 4b but does not change the nature of the intermolecular contacts.

The Inhibitory Caldesmon Peptide LW30 Contains an Extended Sequence and a Well-Defined Turn Configuration. The basis for the ability of the LW30 peptide to form simultaneous attachments of its terminal residues to actin is likely to derive from the conformational properties of the segment that spans the two actin binding sites. The structure of the site-spanning region is reflected in the distance constraints derivable from inspection of the NOE data for LW30.

The $i \rightarrow i+1$ NOE connectivities along the peptide chain of LW30 were broken by the presence of the five proline residues in the sequence whose resonance assignment was readily confirmed by strong $d_{\alpha\delta}$ NOE intensities for each X−Pro dipeptide pair. These $d_{\alpha\delta}$ NOEs identify the trans peptide backbone conformation for each X−Pro pair as also indicated by the characteristic downfield shift of ca. 0.25 ppm for the CH_α resonance of each of the residues preceding proline (*24*). A rigid span of some 2 nm thus characterizes the region of the molecule from Ser-702 to Ser-708 in the LW30 peptide as we have previously demonstrated in the longer peptide 658C (658−756) (*18*).

The peptide chain C-terminal to this elongated segment also displays marked constraints on the backbone dihedral angles adopted. As well as strong $d_{\alpha N}(i, i+1)$ cross-peaks, strong $d_{NN}(i, i+1)$ NOEs occur for residues 708−721, indicative of a structured backbone conformation. These proximities and a variety of clearly resolved nonsequential NOEs characterizing residues 706−717 are shown in Figure 5A. Notable among these medium-range distance indicators

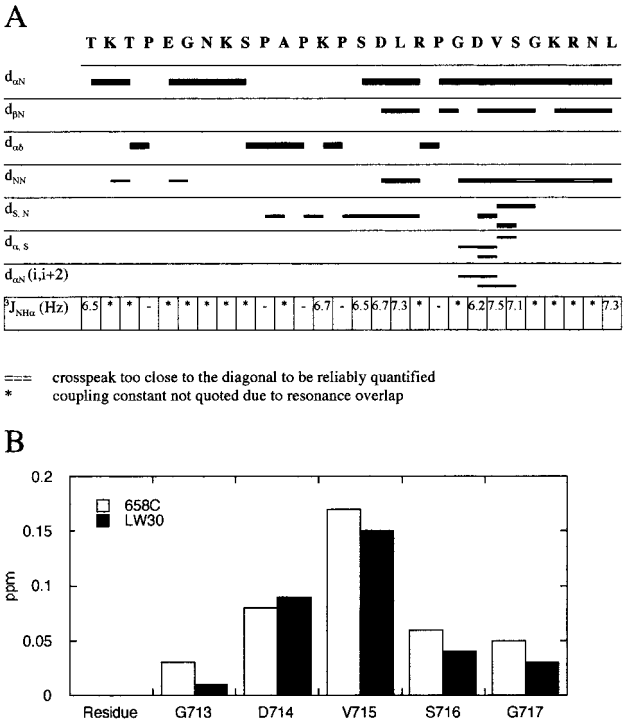

FIGURE 5: (A) Interresidue NOEs observed for different backbone and side chain resonances of the LW30 peptide. Strong, medium, weak, and very weak NOEs are represented by differing widths of the connecting lines indicating proximities between the residues that contain the corresponding groups. The interproton NOEs observed are those between NH (N) and CαH (α) backbone, CβH (β), and side chain (S) resonances. $^3J_{HN\alpha}$ values are given for the amide resonances readily resolvable in the 1D spectrum. (B) Comparison of the CHα chemical shift variation from random coil values (*21*) found for residues 713−717 in LW30 and 658C.

are the $d_{\alpha N}(i, i+2)$ connectivities for Gly-713/Val-715 and Asp-714/Ser-716. This characteristic NOE pattern unambiguously establishes the bend of the peptide chain at this site and indicates a high preference for a β-turn conformation for the Gly-Asp-Val-Ser segment in the sequence. The concurrent observation of strong $d_{NN}(i, i+1)$ connectivities for these residues of LW30 together with the NOEs between the side chain methyls of Val-715 and the backbone amide protons of Asp-714, Ser-716, and Gly-717 provides further confirmatory criteria for the occurrence of a stable backbone turn conformation involving residues 713−716 (Figure 5A).

As well as possessing distinguishing patterns of sequential and medium-range NOEs, β-turns are characterized also by a small value of $^3J_{HN\alpha}$ for residue 2 in the turn (*25*). The observed coupling constant for Asp-714, 6.2 Hz, is indeed smaller than that in the random coil conformation (*26*), and overall the NMR parameters therefore indicate a significantly populated β-turn conformation. This is also illustrated by the good alignment of the superimposed structures derived from the NOE data (Figure 6). The β-turn follows the extended segment (residues 702−707) to provide a well-defined relative orientation of the two flanking actin binding regions.

The Same Structural Elements Spanning the Two Actin Binding Sites Occur in Domain 4b. In light of the results with LW30, we further investigated the structure of the longer domain 4b peptide 658C (658−756). Inspection of the chemical shifts (*18*) and ^{1}H−^{1}H NOE data for the residues of construct 658C linking the actin binding sites

FIGURE 6: Turn conformational preference for the segment $_{713}$Gly-Asp-Val-Ser-Gly$_{717}$ calculated on the basis of the NOE data for these residues. The calibration of NOE intensities was based on the cross-peaks between protons with degenerate autocorrelation peaks according to known secondary structure distances (*25*). Distance constraints for structure calculations were taken from NOESY spectra (250 and 500 ms mixing time). 31 unambiguous sequential and medium-range ($i-j > 1$) interproton distance restraints were derived for the residue segment 713−717. Structures were calculated from the experimental restraints using the X-PLOR program and an extended template structure with ideal covalent geometry. Selection criteria for visualization of the structure were in agreement with the experimental data: no distance violations greater than 0.4 Å, no torsion angle violations greater than 5°, and F_{NOE} less than 180 kJ mol^{-1}. The RMSD for the atoms from the average structure depicted for residues 713−717 was 0.5 Å. Twenty overlayed structures are shown superimposed over the region comprising residues 713−717.

indicates the existence of a restricted conformational average for residues 711−716 (Figure 7). The observed intensity of sequential d_{NN}, $d_{\alpha N}$, and $d_{\beta N}$ cross-peaks for residues 713−716 and the longer range $d_{\alpha N}(i, i+2)$ NOE cross-peaks observed for Gly-713/Val-715 and Asp-714/Ser-716 (Figure 7) match those observed in the spectrum of LW30 (Figure 5) and reflect that the sequence $_{713}$Gly-Asp-Val-Ser$_{716}$ adopts a turn configuration in the intact domain 4b. The characteristic NOE pattern is also matched by similar chemical shift variation for the CHα protons of residues 713−716 for LW30 and the 658C molecule (Figure 5B). The deviation of the chemical shift from random coil values is a qualitative indicator of the conformation and structural flexibility of the corresponding residue sequence (*20*, *21*). The overall retention of the different NMR spectral parameters reinforces the deduction of a turn conformational preference in the region spanning the two actin binding sites of caldesmon domain 4b.

The mutation of the sequence around Trp-692 in the Cg1 mutant of 658C reduces its apparent actin affinity and results in lowered actomyosin ATPase inhibitory potency (*18*). To determine whether these effects are a direct consequence of the substitution in the actin contact sequence or resulted indirectly from an alteration in the conformation of the site-spanning residues, we compared 658C and Cg1. Figure 8 shows the ^{1}H−^{15}N 2D HSQC-TOCSY spectrum of Cg1 labeled with the resonance assignments derived from 3D ^{15}N-separated TOCSY and NOESY experiments. Comparison with data for 658C [above, (*18*), and unpublished] indicates that only localized spectral changes have occurred involving the mutated residues 689−696 with a trans conformation adopted by the introduced Asn−Pro-691 linkage. The conformation of the residues spanning the two sites remains unaltered as judged by the observed retention of chemical shift values, $i \rightarrow i+1$ d_{NN}, $d_{\alpha N}$, $d_{\beta N}$, and $d_{\alpha\delta}$ proximities, and $d_{\alpha N}(i, i+2)$ NOE cross-peak intensity as described above for residues 702−717 of 658C. The lower actin affinity of Cg1 is therefore directly associated with the substitutions introduced at the actin contact sequence.

Domain 4b of Caldesmon Interacts with the C-Terminal Region of Actin. The antagonism of the interaction of LW30 with F-actin by the troponin I peptide (Figure 3) has also been observed with 658C and was suggested to indicate interaction of caldesmon domain 4b at the C-terminus of actin (*18*). To test this proposal, we used peptide fragments of actin to mimic its interaction with caldesmon domain 4b and thus identify residues contributing to the protein interface by NMR. This approach has been validated in a variety of studies of actin binding interactions (*27*, *28*). Of the library of actin peptides titrated with 658C [actin residues 1−18 and 1−28 that interact with the troponin I inhibitory region (*23*), actin residues 16−41, 29−58, 58−84, 96−117, and 350−375], only the peptide derived from the extreme C-terminal of actin provided evidence of interaction.

We investigated the possibility of interaction of LW30 with the peptide comprising actin residues 350−375. Titration of LW30 with the actin peptide was carried out using the minimal concentration of LW30 practicable in order to bias against possible nonspecific binding ($K_b \leq 10^3$ M^{-1}). Addition of the actin peptide resulted in perturbation of the resonances of Thr-694 and Thr-696 (Figure 9A). Unlike the dual contacts formed with F-actin, complex formation between LW30 and actin residues 350−375 did not result in any spectral changes of Leu-721 and Trp-722. Confirmation of the interaction of LW30 with the actin peptide was obtained using Cu^{2+} as a relaxation probe bound to the unique histidine residue, His-371, of the actin peptide. Binding of the cation results in isotropic relaxation effects that vary as r^{-6} from the probe as origin (*29*). Paramagnetic broadening effects on the resonances of Thr-694 and Thr-

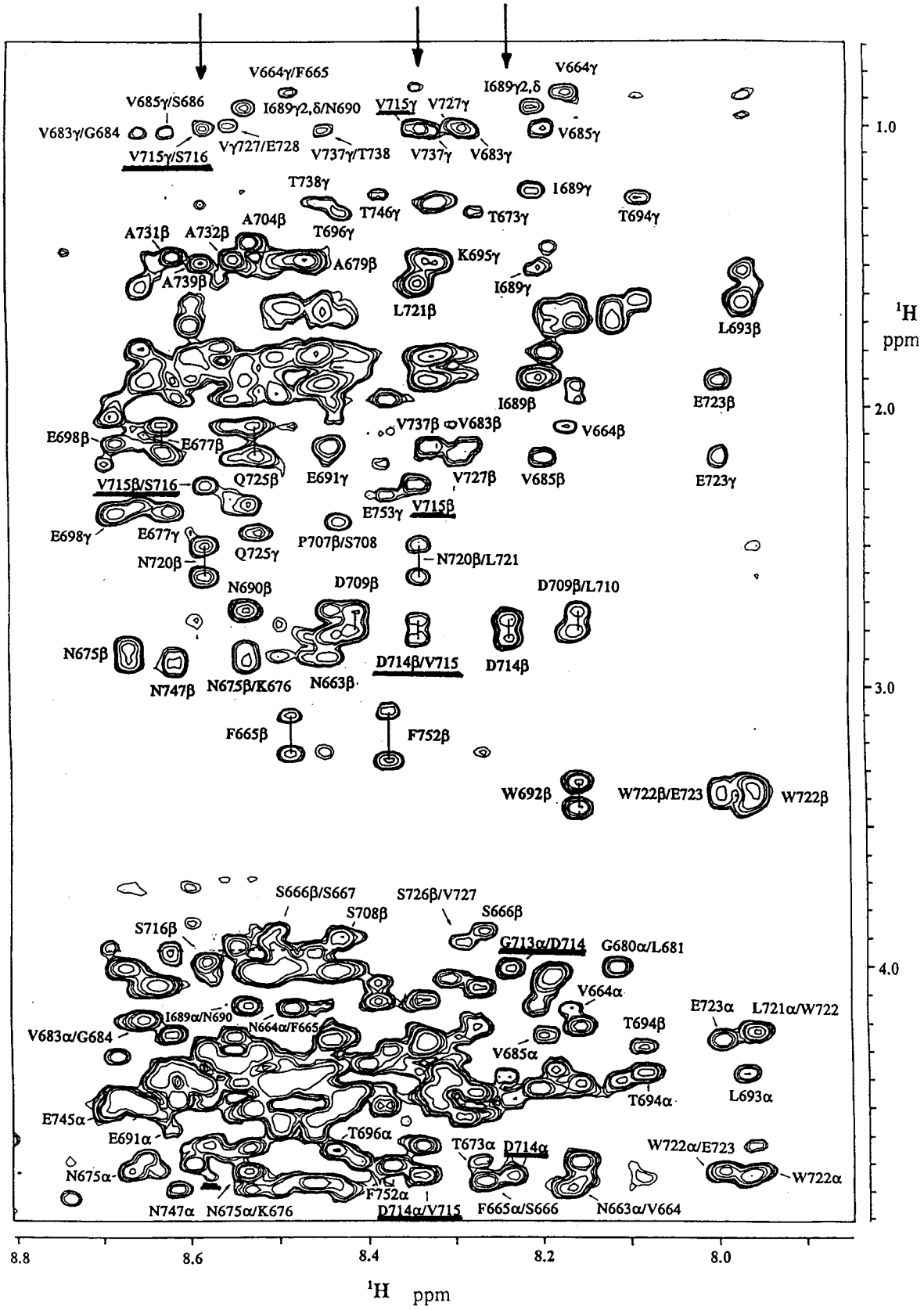

FIGURE 7: Amide spectral region (8−9 ppm) of the ^{1}H 2D NOESY spectrum of 658C (mixing time 110 ms) with cross-peak assignments shown. The amide to α proton and amide to side chain proton cross-peaks for Gly-713, Asp-714, and Val-715 are highlighted.

696 induced by Cu^{2+} bound to the actin peptide indicate that the N-terminal of LW30 is oriented in the vicinity of His-371 (Figure 9B) with no detectable broadening for signals of Leu-721 and Trp-722. The differing proximity to the bound cation of the side chains of Thr-694 and Thr-696 is seen from the greater paramagnetic broadening of the γCH_3 group signal of Thr-696 (Figure 9B). A well-defined geometry therefore exists for the complex of LW30 and actin

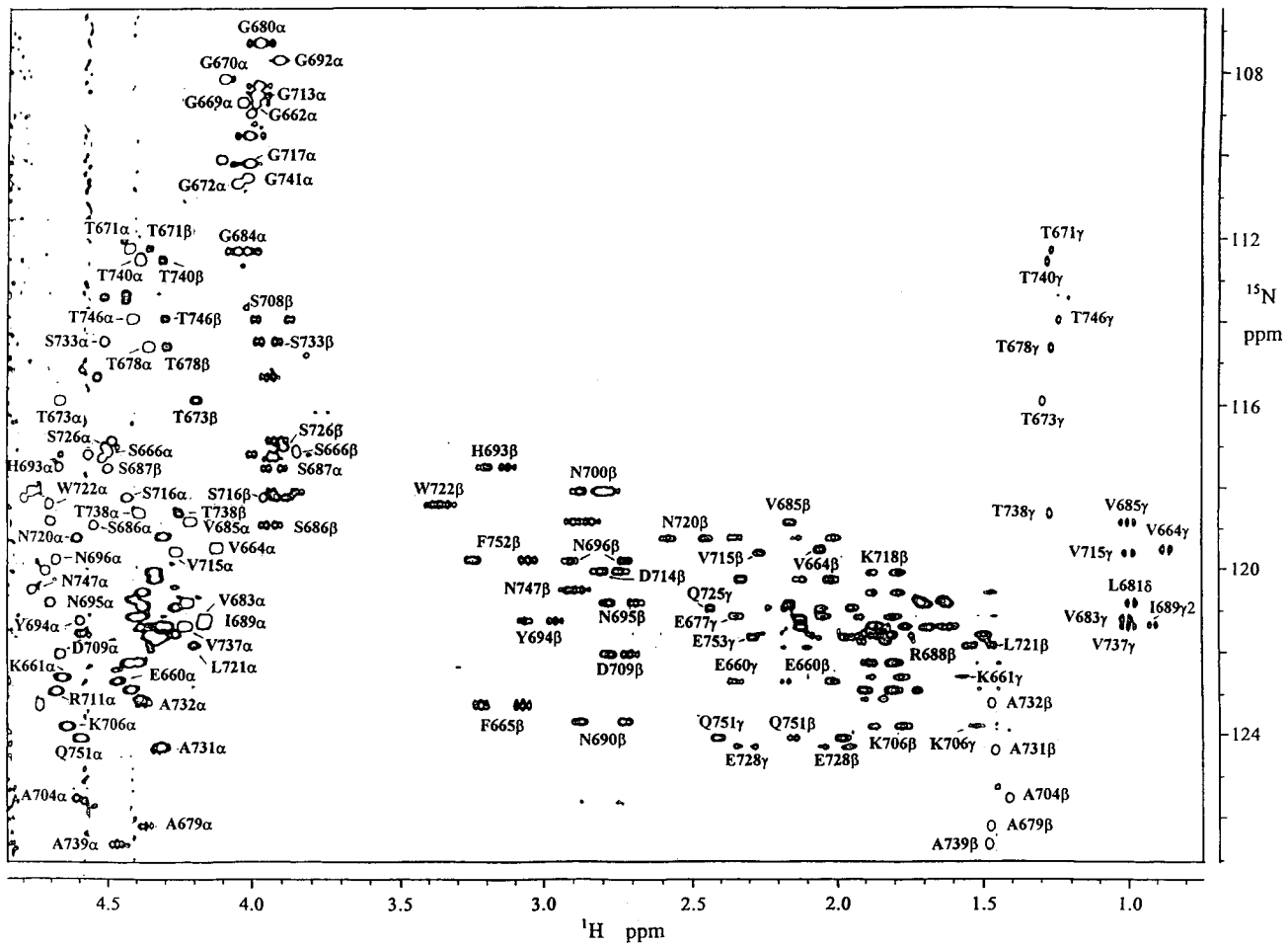

FIGURE 8: Aliphatic region of the $^{1}H-^{15}N$ 2D HSQC-TOCSY spectrum of Cg1 (pH 5.9, $T = 285$ K) showing the spectral resolution of α and side chain proton signals obtained as a result of the dispersion in the ^{15}N chemical shifts.

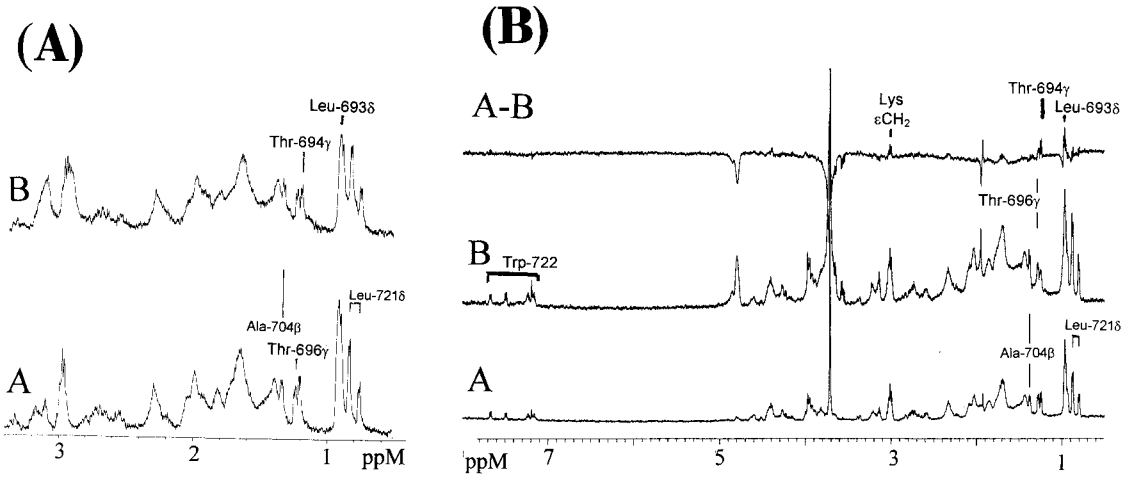

FIGURE 9: (Panel A) Aliphatic region of the proton spectrum (A) of LW30 (50 μM, pH 7.6, $T = 295$ K) and in the presence of 25 μM actin peptide, residues 350−375 (B), obtained upon titration with the actin peptide. (Panel B) Proton spectrum of LW30 in the presence of actin residues 350−375 (150 μM LW30, 25 μM actin peptide, pH 7.6, $T = 295$ K) (trace A) and upon the addition of 10 μM $CuCl_2$ (trace B). The signals of groups of LW30 in the vicinity of the cation bound to His-371 of the actin peptide are highlighted in the difference spectrum shown (A−B).

residues 350−375 (Figure 10).

DISCUSSION

Recent deletion mutant studies and structural analysis have established that the ability of caldesmon to inhibit actomyosin ATPase activity involves the interaction of several nonsequential segments of caldesmon domain 4 with actin (*13, 14, 18*). Two of the three contacts identified are located in the C-terminal half of this region of caldesmon, which has been designated domain 4b. The corresponding expressed peptide (construct 658C, residues 658−756) and two smaller peptides [construct H9, residues 669−737, 726−793 in the human caldesmon sequence; and the LW30 peptide, residues 693−722 (750−779, human sequence)] display inhibitory

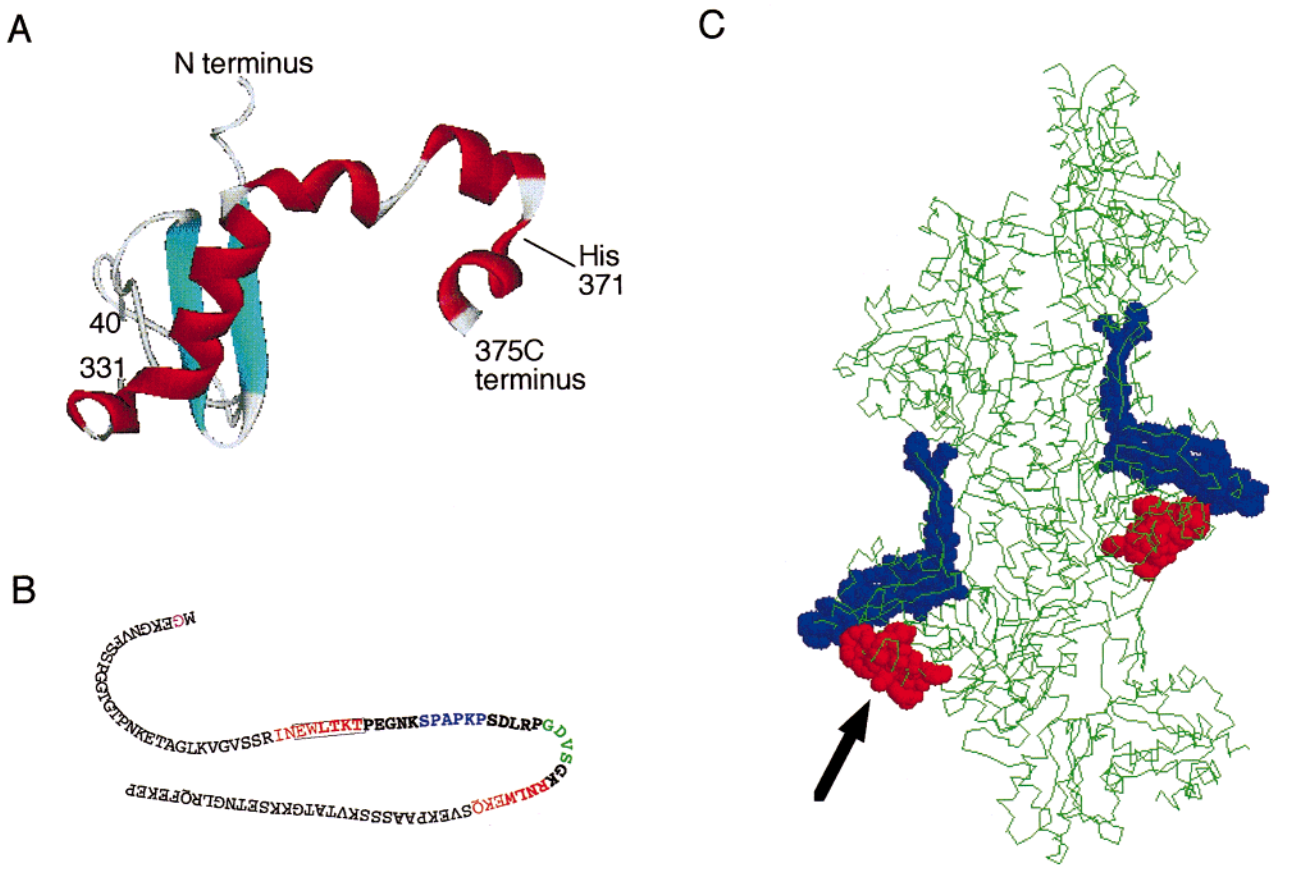

FIGURE 10: (A) Schematic diagram of subdomain 1 of actin showing the topology of the C-terminal residues 331−375 (red) and their location relative to the N-terminal region of actin 1−40 (blue) also on subdomain 1. DNase G-actin structure (*35*) is viewed from the caldesmon domain 4a binding surface showing the proximity of caldesmon and troponin I binding regions. (B) Schematic diagram of caldesmon domain 4b. The 658C sequence is shown with the LW30 segment in boldface. The region mutated in Cg1 is boxed. Amino acids that contact actin are shown in red. The turn is shown in green, and the trans-X−Pro motif is blue. (C) Location of C- and N-terminal peptides in the F-actin structure. C-Terminal (red) and N-terminal (blue) segments are shown in space-filling models superimposed upon the α carbon chains of two actin monomers in a five monomer segment of F-actin. The arrow indicates the approximate direction of view of the peptide structure in (A).

ability enhanced by tropomyosin (*13, 19*). LW30 defines the minimum actin binding inhibitory sequence (Figure 10B). Our results from the studies here of 658C, the 658C mutant Cg1 [sequence $_{691}$Glu-Trp-Leu-Thr-Lys-Thr$_{696}$ changed to Pro-Gly-His-Tyr-Asn-Asn (*18*)], and LW30 indicate that actin interaction with caldesmon domain 4b involves two-pronged docking and that the presence of tropomyosin strengthens the degree of actin association by both contacts. Our results also indicate that the sequence between the two actin contacts adopts a constrained conformation but is not involved in direct interaction with the surface of actin.

The first actin contact segment of domain 4b (Ile-Asn-Glu-Trp$_{692}$-Leu, corresponding to site B) precedes a proline-rich region with a unique sequence (Ser$_{702}$-Pro-Ala-Pro-Lys-Pro) which adopts an extended trans-X−Pro conformation. This is followed by a well-defined turn ($_{713}$Gly-Asp-Val-Ser$_{716}$) immediately adjacent to the second actin contact site (Leu-Trp$_{722}$-Glu-Lys-Gln, site B′) with an overall configuration that resembles a J shape (Figure 10B). The functional relevance of this topology is directly inferred from the inability of peptides containing a single site either alone or in combination to elicit inhibition (*19*). The structure of the linking sequence restricts the spatial disposition of the flanking sites and is both necessary and sufficient to impose a distinct geometry on the two actin contact regions. It is noteworthy that Ser-702, immediately adjacent to the extended proline-rich motif, is the main site for MAPK phosphorylation in caldesmon and is proposed to alter the actin−caldesmon interaction (*30*). The predetermined geometry of interaction could also generate directed conformational change on the surface of actin. This is shown clearly in the case of LW30. The extremities of LW30 are bound to actin, yet each comprises only a part of the actin binding residue sequences associated with each site of domain 4b. Thus, the relative disposition of the two extremities of LW30 enables their simultaneous interaction with actin, and, despite the limited contacts of LW30 with actin, dual-sited interaction results in the inhibition of the ability of actin to productively associate with myosin.

The presence of tropomyosin generates enhanced interaction between caldesmon domain 4b peptides (658C, Cg1, and LW30) and actin in NMR titrations, in agreement with direct binding measurements (*13, 17*−*19*). The associated ability of tropomyosin to potentiate the inhibitory activity of caldesmon domain 4b as well as of LW30 with its limited contacts suggests that the influence of tropomyosin is to alter the conformational equilibrium at the region(s) of actin with which the two sites of caldesmon domain 4b interact. Reciprocally, caldesmon domain 4b would alter the actin−tropomyosin conformational equilibrium; such a conforma-

tional switch has been advocated as the basic mechanism for caldesmon regulation of the thin filament (*11, 31*). Consistent with binding assays which failed to show any affinity of caldesmon domain 4b for tropomyosin (*32*), there was no evidence of any 658C−tropomyosin contacts in the NMR spectra. These observations are in accord with the structural models published by Hodgkinson et al. and Lehman et al. (*33, 34*) which place caldesmon domain 4 and tropomyosin well away from each other in the thin filament.

The interaction of 658C and LW30 with the actin peptide, residues 350−375, indicates that the C-terminal region of actin is involved in the tropomyosin-potentiated inhibition by caldesmon. The C-terminal residues 338−375 of actin are located on subdomain 1. Inspection of the crystallographic structures of actin (*35*) shows that these 37 residues are organized in a helix−turn−helix−strand−helix−turn−helix configuration with the first helical segment (residues 339−350) making stabilizing side chain contacts with residues at the N-terminal of actin (Figure 10). We have demonstrated that caldesmon Thr-694 and Thr-696 (site B) are bound close to His-371 of actin, but the data presented here do not unequivocally identify that both contacts of domain 4b occur at the C-terminal region of actin. This is strongly suggested, however, by the conformation of the site-linking segment. The possibility is consistent with electron microscopy reconstruction (*12, 34*). In this regard, it is noteworthy that the topology of the C-terminus of actin could provide a docking surface complementary to domain 4b of caldesmon. The conformation of this region of actin matches the proposed conformation of the actin binding region of caldesmon domain 4b (Figure 10). Preliminary studies of a peptide (566−669) incorporating domain 4a indicate additional multipoint binding of caldesmon to actin in the regions of Tyr-625 and Trp-659; however, domain 4b and 4a peptides do not interfere with each others interaction with actin as judged from NMR spectra indicating a separate contact site on actin.

There are other actin binding proteins which have some of their contacts at the C-terminus of actin; for instance, the CH domain of calponin and fimbrin contacts 349−352 (*36*) while profilin contacts Arg-372 and Phe-375 (*37, 38*). None of these protein domains have functional similarities with caldesmon, thus emphasizing the importance of the unique multisite docking of caldesmon on actin for inhibition. On the other hand, troponin I, which does have functional similarities with caldesmon (*11, 12*), binds to the N-terminus rather than the C-terminus of actin. The intramolecular contacts connecting the N- and C-termini of actin (Figure 10A) can account for the ability of the short inhibitory peptide of troponin I bound to the N-terminus of actin (*23*) to displace caldesmon domain 4b from the C-terminus of actin. Displacement would be facilitated by small conformational changes distributed through the residues making intramolecular contacts between the N- and C-terminal regions of actin. Since different target regions on actin are associated with the inhibitory activity of the troponin I peptide and that of caldesmon domain 4b, it is evident that regulation by the two molecules involves distinguishable local structural rearrangements. The global cooperative rearrangement of actin−tropomyosin structure involved in switching between on and off states has been shown to include other regions of actin such as Glu-93 (*39*) and Glu_{311}-Arg (*40*). Thus, the possibility remains that different local structural changes can result in a structurally similar large-scale conformational change involved in the control of actin−myosin interaction (*41*).

SUPPORTING INFORMATION AVAILABLE

Proton resonance assignments for the LW30 peptide, caldesmon residues 693−722 (1 page). This material is available free of charge via the Internet at http://pubs.acs.org.

REFERENCES

1. Marston, S. B., and Huber, P. A. J. (1996) in *Biochemistry of Smooth Muscle Contraction* (Barany, M., and Barany, K., Eds.) pp 77−90, Academic Press, San Diego.
2. Marston, S. B., and Smith, C. W. J. (1985) *J. Muscle Res. Cell Motil. 6*, 669−708.
3. Burton, D. J., and Marston, S. B. (1999) *Pflugers Arch. 437*, 267−275.
4. Malmqvist, U., Arner, A., Makuch, R., and Dabrowska, R. (1996) *Pflugers Arch. 432*, 241−247.
5. Dabrowska, R., Goch, A., Galazkiewicz, B., and Osinska, H. (1985) *Biochim. Biophys. Acta 842*, 70−75.
6. Horiuchi, K. Y., Wang, Z., and Chacko, S. (1995) *Biochemistry 34*, 16815−16820.
7. Fraser, I. D. C., and Marston, S. B. (1995) *J. Biol. Chem. 270*, 19688−19693.
8. Marston, S. B., and Redwood, C. S. (1993) *J. Biol. Chem. 268*, 12317−12320.
9. Shirinsky, V., Birukov, K. G., Hettasch, J. M., and Sellers, J. R. (1992) *J. Biol. Chem. 267*, 15886−15892.
10. Chacko, S., and Eisenberg, E. (1990) *J. Biol. Chem. 265*, 2105−2110.
11. Marston, S. B., Fraser, I. D. C., and Huber, P. A. J. (1994) *J. Biol. Chem. 269*, 32104−32109.
12. Marston, S., Burton, D., Copeland, O., Fraser, I., Gao, Y., Hodgkinson, J., Huber, P., Levine, B., EL-Mezgueldi, M., and Notarianni, G. (1998) *Acta Physiol. Scand. 164*, 401−414.
13. Fraser, I. D. C., Copeland, O., Wu, B., and Marston, S. B. (1997) *Biochemistry 36*, 5483−5492.
14. Wang, Z., and Chacko, S. (1996) *J. Biol. Chem. 271*, 25707−25714.
15. Hayashi, K., Kanda, K., Kimizuka, F., Kato, I., and Sobue, K. (1989) *Biochem. Biophys. Res. Commun. 164*, 503−511.
16. Bartegi, A., Fattoum, A., Derancourt, J., and Kassab, R. (1990) *J. Biol. Chem. 265*, 15231−15238.
17. Redwood, C. S., and Marston, S. B. (1993) *J. Biol. Chem. 268*, 10969−10976.
18. Huber, P. A. J., Gao, Y., Fraser, I. D. C., Copeland, O., EL-Mezgueldi, M., Slatter, D. A., Keane, N. E., Marston, S. B., and Levine, B. A. (1998) *Biochemistry 37*, 2314−2326.
19. EL-Mezgueldi, M., Derancourt, J., Callas, B., Kassab, R., and Fattoum, A. (1994) *J. Biol. Chem. 269*, 12824−12832.
20. Spudich, J. A., and Watt, S. (1971) *J. Biol. Chem. 246*, 4866−4871.
21. Brunger, A. T. (1992) *X-PLOR: a system for X-ray crystallography and NMR, version 3.1*, Yale University Press, New Haven, CT.
22. Smith, C. W., Pritchard, K., and Marston, S. B. (1987) *J. Biol. Chem. 262*, 116−122.
23. Levine, B. A., Moir, A. J. G., and Perry, S. V. (1988) *Eur. J. Biochem. 172*, 389−397.
24. Chavanieu, A., Keane, N. E., Quirk, P. G., Levine, B. A., Calas, B., Wei, L., and Ellis, L. (1994) *Eur. J. Biochem. 224*, 115−123.
25. Wüthrich, K. (1986) *NMR of proteins and nucleic acids*, Wiley, New York.
26. Smith, L. J., Bolin, K. A., Schwalbe, H., MacArthur, M. W., Thornton, J. M., and Dobson, C. M. (1996) *J. Mol. Biol. 255*, 494−506.

27. Friederich, E., Vancomperelle, K., Huet, C., Goethals, M., Finidori, J., Vandekerkhove, J., and Louvard, D. (1992) *Cell 70*, 81−92.
28. Levine, B. A., Moir, A. J. G., Patchell, V. B., and Perry, S. V. (1992) *FEBS Lett. 298*, 44−48.
29. Dwek, R. A. (1973) *NMR in Biochemistry*, Clarendon Press, Oxford.
30. Adam, L. P. (1996) in *Biochemistry of smooth muscle contraction* (Barany, M., Ed.) pp 167−180, Academic Press, San Diego.
31. Lehrer, S. S., and Geeves, M. A. (1998) *J. Mol. Biol. 277*, 1081−1089.
32. Huber, P. A. J., Fraser, I. D. C., and Marston, S. B. (1995) *Biochem. J. 312*, 617−625.
33. Lehman, W., Vibert, P., and Craig, R. (1997) *J. Mol. Biol. 274*, 310−317.
34. Hodgkinson, J. L., Marston, S. B., Craig, R., Vibert, P., and Lehman, W. (1997) *Biophys. J. 72*, 2398−2404.
35. Kabsch, W., Mannherz, H. G., Suck, D., Pai, E. F., and Holmes, K. C. (1990) *Nature 347*, 37−44.
36. Hodgkinson, J. L., EL-Mezgueldi, M., Craig, R., Vibert, P., Marston, S. B., and Lehman, W. (1997) *J. Mol. Biol. 273*, 150−159.
37. Schutt, C. E., Myslik, J. C., Rozycki, M. D., Goonsekere, N. C., and Lindberg, U. (1993) *Nature 365*, 810−816.
38. Rozycki, M. D., Myslik, J. C., Schutt, C. E., and Lindberg, U. (1994) *Curr. Opin. Cell Biol. 6*, 87−95.
39. Bing, W., Razzaq, A., Sparrow, J., and Marston, S. (1998) *J. Biol. Chem. 273*, 15016−15021.
40. Saeki, K., Sutoh, K., and Wakabayashi, T. (1996) *Biochemistry 35*, 14465−14472.
41. Dobrowolski, Z., Borovikov, Y. S., Nowak, E., Galazkiewicz, B., and Dabrowska, R. (1988) *Biochim. Biophys. Acta 956*, 140−150.

BI991383K